


Cite this: *RSC Adv.*, 2020, 10, 10017

# Constructing a TiO<sub>2</sub>/PDA core/shell nanorod array electrode as a highly sensitive and stable photoelectrochemical glucose biosensor†

Wei Xu,<sup>a</sup> Wenke Yang,<sup>a</sup> Hongkai Guo,<sup>a</sup> Lianyan Ge,<sup>a</sup> Jinchun Tu<sup>✉</sup><sup>\*,a</sup> and Chao Zhen<sup>\*,b</sup>

Developing stable PEC glucose biosensors with high sensitivity and low detection limit is highly desirable in the biosensor field. Herein, a highly stable and sensitive enzymatic glucose photoelectrochemical biosensor is rationally designed and fabricated by constructing TiO<sub>2</sub>/PDA core/shell nanorod arrays. The TiO<sub>2</sub> nanorod as the core has the advantages of increasing charge transportation towards interfaces and enhancing the absorption of incident sunlight due to its single-crystal nature and one dimensional array structure. The PDA shell not only induces a rapid charge transfer across the interfaces but also stabilizes the biosensor performance by avoiding the decomposition of enzymes induced by the strong oxidizing holes from the TiO<sub>2</sub> core. A remarkable performance with an ultrahigh sensitivity of 57.72  $\mu\text{A mM}^{-1} \text{cm}^{-2}$ , a linear range of 0.2–1.0 mM, a glucose detection limit of 0.0285 mM (S/N = 3) and a high sensitivity of 8.75  $\mu\text{A mM}^{-1} \text{cm}^{-2}$  in a dynamic range of 1.0–6.0 mM were obtained for the glucose detection. This study might provide a strategy for constructing inorganic/organic core/shell structures with a satisfactory PEC performance.

Received 12th December 2019

Accepted 16th February 2020

DOI: 10.1039/c9ra10445c

rsc.li/rsc-advances

## 1. Introduction

Glucose is a simple sugar that widely exists in the blood of living organisms. The efficient detection of glucose is important in terms of health applications.<sup>1–3</sup> Photoelectrochemical (PEC) bioanalysis has emerged as a promising analytical technique for applications in numerous fields with special emphasis on immunoassays, enzymatic biosensing and cell-related detections due to its low cost, lower background interference and high sensitivity.<sup>4–7</sup> Since the photoelectrode for PEC detection performs the tasks of capturing light, generating charge carriers and inducing surface chemical reactions, choosing suitable photoactive materials is critical for the construction of high-efficiency PEC biosensors. TiO<sub>2</sub> with the merits of being non-toxic, with favorable band alignments, good stability, cost-effectiveness and biocompatibility, has been regarded as

a promising candidate material for the construction of PEC biosensors.<sup>8–10</sup> Its drawbacks include having a poor charge carrier transport ability and high oxidative activity of photo-generated holes as a result of the deep valence band edge position, which may lead to the decomposition of the target.<sup>11</sup>

One-dimensional (1D) single crystal arrays, which favor electron transport along the axial direction and shorten the hole diffusion length towards the surface along the radial direction, have been considered as advantageous structures for PEC applications. A series of methods have been used to enhance the performance of PEC glucose biosensors based on 1D TiO<sub>2</sub> single crystal arrays by constructing heterostructures to promote the charge separation (*e.g.*, CdS/TiO<sub>2</sub> heterostructure,<sup>12</sup> Au@TiO<sub>2</sub>,<sup>13</sup> and MoS<sub>2</sub> nanosheet-TiO<sub>2</sub> nanorod heterostructure<sup>14</sup>). The area and quality of the interface are two important factors affecting the performance of PEC glucose biosensors. 1D core-shell heterostructures have the advantage of achieving a full interface contact between two components along with unique optoelectronic properties<sup>15</sup> to construct efficient PEC biosensors.<sup>16</sup> Moreover, the shell can act as dispersant and intermediate layer,<sup>17</sup> suppressing the aggregation of active materials. Considering the advantages of the 1D core/shell structure in improving charge transfer across interfaces, it is highly desirable to construct 1D core/shell structure-based PEC biosensors.

Poly-dopamine (PDA) as a p-type semiconductor<sup>18</sup> contains the proper band edges to construct type II heterostructures using TiO<sub>2</sub>. The surface hydroxyl groups of TiO<sub>2</sub> can react with the catechol groups of PDA to form a bridged bidentate bond as

<sup>a</sup>State Key Laboratory of Marine Resource Utilization in South China Sea, College of Materials and Chemical Engineering, Hainan University, Haikou 570228, China. E-mail: tujinchun@hainu.edu.cn

<sup>b</sup>Shenyang National Laboratory for Materials Science, Institute of Metal Research, Chinese Academy of Sciences, 72# Wenhua RD, Shenyang 110016, China. E-mail: czhen@imr.ac.cn

† Electronic supplementary information (ESI) available: XRD patterns and FTIR spectra of the TiO<sub>2</sub> nanorod arrays and TiO<sub>2</sub>/PDA core/shell nanorod arrays; chronoamperometric *i*-*t* response of glucose oxidase modified TiO<sub>2</sub>/PDA electrode to glucose; chronoamperometric *i*-*t* response of the glucose oxidase modified TiO<sub>2</sub> electrode and its calibration curve; stability test of the glucose oxidase modified TiO<sub>2</sub>/PDA electrode. See DOI: 10.1039/c9ra10445c



direct electron transfer channels between PDA and  $\text{TiO}_2$ .<sup>19</sup> Moreover, PDA as a p-type semiconductor provides a strong adsorption ability between the electrode materials and enzymes.<sup>20</sup> Moreover, using PDA as a shell component not only promotes the separation of photogenerated charge carriers but also avoids the decomposition of enzymes induced by the high oxidative holes generated by the  $\text{TiO}_2$  core under light irradiation. Here, a photoelectrode based on  $\text{TiO}_2$ /PDA core/shell nanorod arrays with rapid interface transfer has been constructed as a stable highly sensitive PEC glucose biosensor (Scheme 1). The resulting PEC biosensor can deliver an ultra-high sensitivity of  $57.72 \mu\text{A mM}^{-1} \text{cm}^{-2}$ , a linear range of 0.2–1 mM with a glucose detection limit of 0.0285 mM ( $S/N = 3$ ) and a high sensitivity of  $8.75 \mu\text{A mM}^{-1} \text{cm}^{-2}$  for a dynamic range of 1–6 mM for glucose detection.

## 2. Experimental

### 2.1 Fabrication of $\text{TiO}_2$ nanorod arrays

Prior to the growth of  $\text{TiO}_2$  nanorod arrays, FTO glass substrates were ultrasonically cleaned in isopropanol, acetone and distilled water, each for 20 min. Nanorod arrays were grown referring to the previous report.<sup>21</sup> In a typical process, the transparent precursor solution containing 13 mL of hydrochloric acid (38 wt%), 15 mL of deionized water and 440  $\mu\text{L}$  of tetrabutyl titanate was transferred into a Teflon-lined autoclave with a volume of 50 mL and the FTO substrate was introduced in the solution. The autoclave was kept in an oven at  $150^\circ\text{C}$  for 10 h. After cooling to room temperature, the FTO glass was rinsed with deionized water and ethanol several times. Finally, it was air-dried and annealed at  $400^\circ\text{C}$  for 2 h with a heating rate of  $2^\circ\text{C min}^{-1}$ .

### 2.2 Synthesis of $\text{TiO}_2$ /PDA core/shell nanorod arrays

The PDA shell was coated on  $\text{TiO}_2$  nanorods *via* an aqueous chemical growth method. 10 mg of hexamethylene tetraamine (HMTA) and 1 mg of dopamine hydrochloride were dissolved in 40 mL deionized water. 1 mL of this solution was dropwise added to 48 mL of deionized water under stirring, and the solution obtained was then transferred to a 50 mL conical

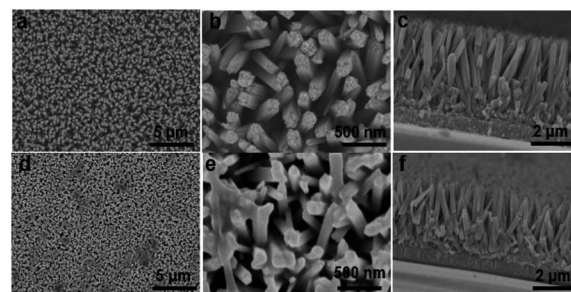


Fig. 1 SEM images: (a and b) top-view of  $\text{TiO}_2$  nanorod arrays; (c) cross-section view of  $\text{TiO}_2$  nanorod arrays; (d and e) top-view of  $\text{TiO}_2$ /PDA core/shell nanorod arrays; (f) cross-section view of  $\text{TiO}_2$ /PDA core/shell nanorod arrays.

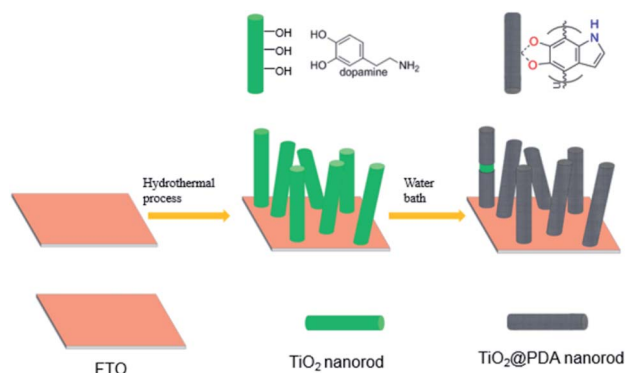
flask. The FTO substrate-supported  $\text{TiO}_2$  nanorod arrays were put into the above conical flask, which was kept in a water bath at  $90^\circ\text{C}$  for 3 h. After cooling to room temperature, the  $\text{TiO}_2$  nanorod arrays were rinsed with deionized water and dried in air. The PDA powder reference sample was synthesized using similar procedures without introducing the FTO substrate-supported  $\text{TiO}_2$  nanorod arrays.

### 2.3 Fabrication of the PEC electrode

The glucose oxidase-modified  $\text{TiO}_2$ /PDA biosensor was obtained as follows. 10  $\mu\text{L}$  of a  $10 \text{ mg mL}^{-1}$  aqueous solution of glucose oxidase solution (glucose oxidase was dispersed in phosphate-buffered saline,  $\text{pH} = 7.4$ ) was first stirred in a thermostated oscillator at  $4^\circ\text{C}$  for 4 h. Then, 10  $\mu\text{L}$  of this solution was dropped on the FTO substrate-supported  $\text{TiO}_2$ /PDA electrode and dried at  $4^\circ\text{C}$  for 8 h.

### 2.4 Characterization

X-ray diffraction (XRD) patterns were recorded on a diffractometer (BrukerD8) using  $\text{Cu K}\alpha$  as the irradiation source. The



Scheme 1 Diagram of the synthesis of  $\text{TiO}_2$ /PDA core shell nanorod arrays on fluorine transparent oxide (FTO) glass substrates.

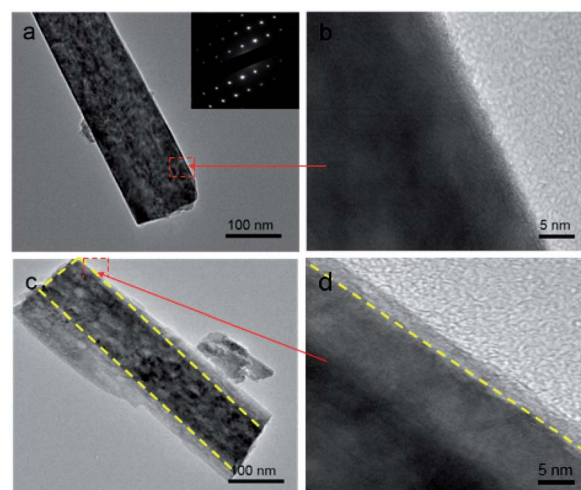


Fig. 2 Low-magnification TEM images of a nanorod scraped from (a) pristine rutile  $\text{TiO}_2$  nanorod arrays (SAED in the inset) and (c)  $\text{TiO}_2$ /PDA core/shell nanorod arrays; (b and d), enlarged images from the areas marked by the red rectangles in (a) and (c).



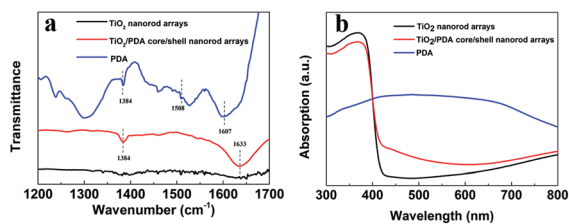


Fig. 3 (a) FTIR spectra and (b) UV-vis absorption spectra of TiO<sub>2</sub> nanorod arrays, PDA and TiO<sub>2</sub>/PDA core/shell nanorod arrays.

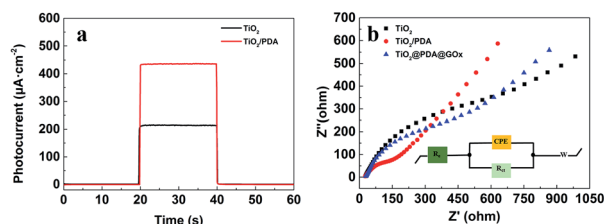


Fig. 4 (a) Photocurrent response and (b) EIS Nyquist plots of TiO<sub>2</sub> (black line) and TiO<sub>2</sub>/PDA (red line) samples in 0.1 M PBS (pH = 7.4) (the blue-dashed line is the EIS Nyquist plot of the photoelectrode).

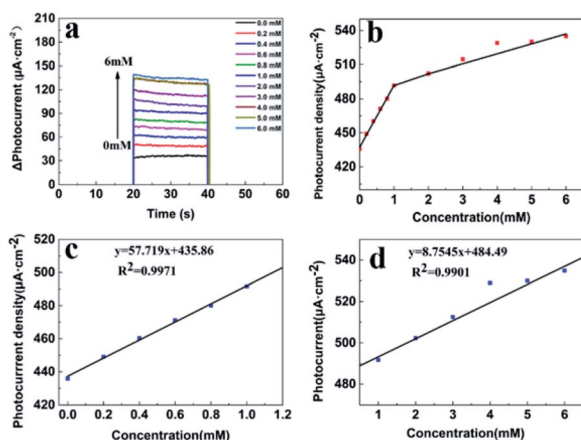


Fig. 5 (a) Chronoamperometric  $\Delta i$ - $t$  response of the glucose oxidase modified TiO<sub>2</sub>/PDA electrode to the glucose at different concentrations in phosphate buffer at 0.4 V; (b) calibration curves of glucose concentration and photocurrent density; (c) and (d) are two linear curves within different glucose concentration ranges shown in (b).

morphology of the PEC electrode was characterized *via* scanning electron microscopy using a microscope (Hitachi SU8010). The structure was determined *via* transmission electron microscopy (TEM) using a microscope (JEOL JEM 2100). UV-vis absorption spectra were recorded on a UV-vis absorption spectrophotometer (Persee, TU-1901). Fourier transform infrared (FTIR) spectra were recorded on a Bomem MB 100 FT-IR spectrometer (ABB Bomem, QC, Canada).

## 2.5 PEC sensing measurements

PEC tests were performed in a three-electrode electrochemical system, where a Pt foil, glucose oxidase modified TiO<sub>2</sub>/PDA

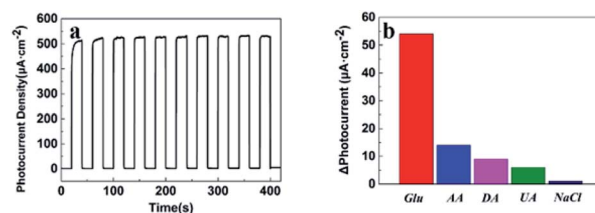


Fig. 6 (a) Stability test of the glucose oxidase modified TiO<sub>2</sub>/PDA electrode at the concentration of 1 mM glucose; (b) amperometric response of the glucose oxidase modified TiO<sub>2</sub>/PDA electrode to the addition of glucose (Glu, 1 mM); ascorbic acid (AA, 0.1 mM); dopamine (DA, 0.1 mM); uric acid (UA, 0.1 mM) and NaCl (0.1 mM). All tests were performed at an applied voltage of 0.4 V in 0.1 M of PBS (pH = 7.4).

photoelectrode and Ag/AgCl electrode were used as the counter electrode, working electrode and reference electrode, respectively. Phosphate-buffered saline (PBS, pH = 7.4) was used as the electrolyte. PEC tests were performed on a CHI 660C workstation (CHI Instruments, Chenhua, Shanghai, China). The active area of the sensor exposed to the electrolyte is approximately 1 cm<sup>2</sup>. During the PEC tests, different volumes of glucose were injected into the electrolyte solution. The photoelectrode was illuminated under a Xe-lamp (AM 1.5 G, 100 mW cm<sup>-2</sup>). To optimize the photocurrent as well as to minimize possible side electrochemical reactions, a bias of 0.4 V (vs. Ag/AgCl) was applied.

## 3. Results and discussion

Fig. 1a and b show typical top-view SEM images of the hydrothermally grown TiO<sub>2</sub> nanorod arrays with different magnifications. The FTO substrate surface is uniformly covered with ordered nanorods. The nanorods have four smooth lateral surfaces and rough quasi-square top. The average width of the nanorods was around 100 nm. The image showing the cross-section view demonstrates that the nanorods intimately stand on the FTO substrate (Fig. 1c), facilitating the charge transport along the rod axis.<sup>22</sup> Coating the nanorods with the PDA structure does not change the basic morphology of the nanorods but leads to smoother nanorod tops (Fig. 1d and e). The cross-section view of the resultant TiO<sub>2</sub>/PDA core/shell sample further demonstrates the preservation of the nanorods (Fig. 1f), suggesting that the PDA shell is uniformly coated on the TiO<sub>2</sub> nanorods. The film thickness of both TiO<sub>2</sub> and TiO<sub>2</sub>/PDA nanorods was measured to be ~2.5 μm from their cross-section SEM images (Fig. 1c and f). The thin PDA shell is beneficial for immobilizing the enzyme.<sup>23</sup> The crystal structure of the samples was studied by recording their XRD patterns (Fig. S1†). Diffraction peaks at 26.5, 33.8, 37.9, 51.7, 61.7 and 65.8 degrees are assigned to the rutile phase of SnO<sub>2</sub> from the FTO substrates (JCPDS no. 77-0451). The diffraction peaks at 36.1, 54.3, 62.7, 69.0, 69.8 and 76.5 correspond to the rutile phase of TiO<sub>2</sub> (JCPDS no. 02-0494). After modifying the PDA shell, no additional peak was detected due to its low loading amount and polymeric nature.

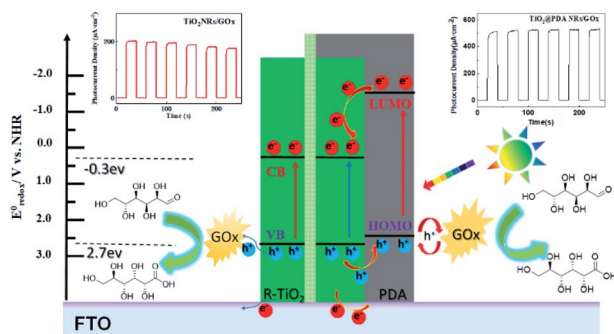
In order to confirm the formation of the PDA shell, the microstructures of a single nanorod scrapped from the TiO<sub>2</sub> and





Table 1 Comparison of the analytical performance of PEC glucose biosensors

GOx PEC biosensors	Dynamic range (mM)	Detection limit (mM)	Sensitivity ( $\mu\text{A mM}^{-1} \text{cm}^{-2}$ )	Reference
TiO <sub>2</sub> /PDA/GOx	0.2–1, 1.00–6.00	0.0285	57.72, 8.75	This work
GOx/SnS <sub>2</sub> /Nafion/GCE	0.025–1.10	0.01	7.6	37
ITO/MoS <sub>2</sub> -TiO <sub>2</sub> /GOx	0.100–10.0	0.015	0.81	14
ITO/SnO <sub>2</sub> /Ag <sub>2</sub> S/GOx	0.100–12.2	0.032	0.029	38
Nafion/GOx/Ag-Pdop@CNT/GCE	0.050–1.10	0.017	3.1	39
GOx/TCS-TiO <sub>2</sub> /chitosan/GCE	0.005–1.32	0.002	23.2	40
ITO/TiO <sub>2</sub> -Co <sub>3</sub> O <sub>4</sub> -CNT-GOx	0.000–4.00	0.00016	0.3	41

Scheme 2 Mechanism of the PEC detection of glucose at glucose oxidase-modified TiO<sub>2</sub> (left panel) and TiO<sub>2</sub>/PDA (right panel) electrodes.

TiO<sub>2</sub>/PDA core/shell nanorod arrays were characterized *via* TEM. The TiO<sub>2</sub> nanorod has a width of  $\sim 100$  nm (Fig. 2a), which is in accordance with the SEM results (Fig. 1b). The selected-area electron diffraction (SAED) pattern recorded from the TiO<sub>2</sub> nanorod (the inset in Fig. 2a) shows periodic spots, indicating the single-crystalline feature of the as-prepared rutile TiO<sub>2</sub> nanorods. This can be further demonstrated from the high-resolution TEM (HR-TEM) image (Fig. 2b). The width of the nanorod from the TiO<sub>2</sub>/PDA core-shell arrays becomes larger (Fig. 2c). Compared to the pristine one (Fig. 2b), the TiO<sub>2</sub> nanorod is homogeneously coated with an amorphous PDA shell (Fig. 2d). The HR-TEM image reveals the high quality interface structure between the TiO<sub>2</sub> core and the PDA shell. This is largely caused by strong interactions between the hydroxyl groups on the TiO<sub>2</sub> surface and the catechol group of the DA unit, leading to the formation of a bridged bidentate bond between the TiO<sub>2</sub> core and the PDA shell.<sup>24</sup>

To further confirm the nature of the amorphous PDA layer, Fourier transform infrared (FTIR) spectra of the PDA, TiO<sub>2</sub> and TiO<sub>2</sub>/PDA core/shell nanorod arrays (Fig. 3a) were recorded. TiO<sub>2</sub> nanorod arrays have an obvious band at  $1633 \text{ cm}^{-1}$ , which is originated from the deformational vibration of the H–O–H bonds from absorbed water molecules.<sup>25</sup> The peaks at  $1508 \text{ cm}^{-1}$  and  $1607 \text{ cm}^{-1}$  for the PDA sample correspond to the vibration models of indole or indoline structures in PDA.<sup>26</sup> Moreover, the peak at  $3410 \text{ cm}^{-1}$  derived from the catechol OH group is also an evidence for the existence of PDA (Fig. S2†). Compared to TiO<sub>2</sub>, an additional sharp peak at  $1384 \text{ cm}^{-1}$ , derived from the vibrations of CH or substituents of the

benzene ring, is formed in the spectrum of the TiO<sub>2</sub>/PDA sample. In addition, the enhanced absorption peaks at around  $1630 \text{ cm}^{-1}$  and  $3440 \text{ cm}^{-1}$  suggest the increased absorption ability of water molecules from the TiO<sub>2</sub>/PDA sample. UV-vis absorption spectra of different samples are compared in Fig. 3b. A bandgap of  $\sim 3.0$  eV for the TiO<sub>2</sub> sample was determined by plotting the Kubelka–Munk function *versus* the energy. The PDA sample has a strong absorption band in the range from 300 to 800 nm. This can be understood as the result of the p-conjugated polymer chains of PDA that facilitates the separation of the photogenerated carrier due to its high molar absorption coefficient in the wide spectral region of sunlight.<sup>27,28</sup> The TiO<sub>2</sub>/PDA sample shows a slight absorption enhancement in the whole visible range. The intrinsic absorption edge of TiO<sub>2</sub> shows no change with the introduction of PDA.

In order to show the optimum potential better, first, we performed the *J*–*V* curve test within the potential range from  $-0.4$  to  $0.4$  V (Fig. S3†). Subsequently, the photocurrent measurements of the TiO<sub>2</sub> and TiO<sub>2</sub>/PDA electrodes were used to evaluate their potential as the PEC biosensors. As shown in Fig. 4a, both TiO<sub>2</sub> and TiO<sub>2</sub>/PDA samples showed a negligible amount of current in dark, which means low-noise. The photocurrent density of TiO<sub>2</sub> and TiO<sub>2</sub>/PDA electrodes experiences a substantial increase under illumination. The photocurrent density of the TiO<sub>2</sub>/PDA electrode is about twice as high as that of the TiO<sub>2</sub> electrode. The great improvement of the photocurrent density stems from the introduction of the PDA shell that has formed the high-quality interface with the TiO<sub>2</sub> core. The photoelectrons generated in the PDA shell can effectively be transferred from its conduction band to that of the TiO<sub>2</sub> nanorod core due to the type II band edge alignment and strong chemical bonding dominating the interface structure. The photo-holes generated in the TiO<sub>2</sub> nanorod core can effectively be transferred from its valence band (VB) to that of the PDA shell. These transfers promote an efficient separation of the photogenerated electrons and holes between the TiO<sub>2</sub> core and the PDA shell. The results demonstrate the higher photo-sensitivity of the core-shell structure.

To get further insight into the dynamics of the charge transfer, electrochemical impedance spectroscopy (EIS) was performed on the different samples. The EIS measurements were conducted in a PBS buffer within a frequency range from 100 kHz to 0.1 Hz, and an AC perturbation of 36 mV (Fig. 4b).



Nyquist EIS spectra are commonly composed of two parts. One is a semicircle at a high frequency region that reflects the charge transfer process. Its radius is defined as the transfer resistance ( $R_{ct}$ ) across interfaces. The other is a line plot at a lower frequency range that corresponds to the diffusion process.<sup>29</sup> The equivalent circuit (the inset in Fig. 4b) is used to fit the Nyquist plots recorded from different samples, where  $R_e$  is the system resistance, CPE represents the capacitive phase at the interface between the electrolyte and photoelectrode, the  $R_{ct}$  stands for the charge carrier transfer resistance across the interface, and  $W$  is the diffusion resistance. The fitted  $R_{ct}$  (403.8  $\Omega$ ) of the  $\text{TiO}_2$  sample is much larger than that of the  $\text{TiO}_2/\text{PDA}$  sample (65.9  $\Omega$ ). The  $R_{ct}$  (234.4  $\Omega$ ) of the glucose oxidase modified  $\text{TiO}_2/\text{PDA}$  sample is much smaller than that of the  $\text{TiO}_2$  sample, indicating that the introduction of the PDA shell facilitates the charge carrier transfer process and enhances the reaction kinetics due to the intimate interface between the PDA shell and the  $\text{TiO}_2$  core by forming a bridged bidentate bond to effectively reduce the interface resistance.

Fig. 5a displays the chronoamperometric  $\Delta i-t$  response of the glucose oxidase modified  $\text{TiO}_2/\text{PDA}$  electrode at 0.4 V (vs. Ag/AgCl) in a buffered solution of different glucose concentrations under continuous stirring (the unabridged chronoamperometric  $i-t$  response of the electrode is given in Fig. S4†). Fig. 5c shows that the glucose oxidase modified  $\text{TiO}_2/\text{PDA}$  electrode exhibits a good photocurrent response to the detection of glucose in the concentration range of 0.2–1 mM with an ultra-sensitivity of 57.72  $\mu\text{A mM}^{-1}$  and a low detection limit of 0.0285 mM. The limit of detection (LOD) was calculated through the formula,  $\text{LOD} = 3S_b/S$  (where  $S_b$  is the standard deviation of 10 blank measurements and  $S$  is the sensitivity). The limit of quantification (standard deviation of 10 blank measurements/sensitivity) was estimated to be 0.095 mM.<sup>30,41</sup> However, pure  $\text{TiO}_2$  nanorod array electrodes (Fig. S5†) have a much lower detection sensitivity of 20.85  $\mu\text{A mM}^{-1}$  in the same detection range and the higher detection limit of 0.081 mM ( $S/N = 3$ ) for glucose. Interestingly, there are two linear ranges of the glucose oxidase modified  $\text{TiO}_2/\text{PDA}$  electrode for quantifying glucose in the concentration range from 0.2–1.0 mM and 1.0–6.0 mM (Fig. 5b). The linear dependence of the oxidation currents on the glucose concentration from 0.2 to 1.0 mM and from 1.0 to 6.0 mM in Fig. 5c and d, display a correlation coefficient ( $R_2$ ) of 0.9971 and 0.9901, respectively. The sensitivity for this electrode was determined to be 57.72  $\mu\text{A mM}^{-1}$  and 8.75  $\mu\text{A mM}^{-1}$ , respectively. The limit of detection (LOD) for glucose detection was calculated to be 0.0285 mM ( $S/N = 3$ ), suggesting an excellent PEC performance of the sensors. The presence of two linear regions may be ascribed to the adsorption of intermediates. Under the condition of low glucose concentrations, the linear relationship shows a steep slope because the glucose molecules can freely diffuse towards the electrode. In contrast, under the condition of a high glucose concentration, the interactions between glucose molecules become stronger, decreasing the curve slope.<sup>31</sup>

The stability of the glucose oxidase-modified  $\text{TiO}_2/\text{PDA}$ -based PEC biosensor was evaluated by recording the time-dependent photocurrent for 10 light irradiation on/off cycles

in the presence of 1 mM glucose, as shown in Fig. 6a. The enediol ligands of PDA have a high stability toward oxidation after forming the bidentate bonds with  $\text{TiO}_2$  nanorods, thus the degradation of PDA can be avoided.<sup>32</sup> These results show the high stability of the photocurrent of the glucose oxidase-modified  $\text{TiO}_2/\text{PDA}$  ( $\text{TiO}_2/\text{PDA}/\text{GOx}$ )-based PEC biosensor. In contrast, a significant photocurrent attenuation for glucose oxidase-modified  $\text{TiO}_2$  nanorod arrays is observed in the time-dependent photocurrent because of the photogenerated holes that have a strong oxidation ability in  $\text{TiO}_2$  and cause the deactivation of the enzyme (Fig. S6†). To explore the specificity of the PEC biosensor, several interfering compounds, such as ascorbic acid (AA), dopamine (DA), NaCl and uric acid (UA) were introduced along with glucose (Glu), as displayed in Fig. 6b. The PEC biosensor shows an excellent anti-interference performance. Comparison of the analytical performance of the PEC glucose biosensors listed in Table 1 shows acceptable results in terms of the linear relationship range and detection sensitivity.

The excellent behavior of the glucose oxidase-modified  $\text{TiO}_2/\text{PDA}$ -based biosensor is attributed to the following plausible mechanism shown in Scheme 2. The PDA absorbs photons with enough energy to induce a  $\pi-\pi^*$  transition under the irradiation of light. The electrons in the excited-state jump from the highest occupied molecular orbital (HOMO) of PDA to its lowest unoccupied molecular orbital (LUMO). The conduction band potential ( $E_{CB}$ ) of the rutile  $\text{TiO}_2$  is about  $-0.3$  eV (vs. NHE), whereas the LUMO potential of PDA is  $-1.468$  eV (vs. NHE).<sup>33,34</sup> Therefore, the photogenerated electrons in the HOMO of PDA flow thermodynamically quicker to the conduction band of the rutile  $\text{TiO}_2$ . The single crystalline nature of rutile  $\text{TiO}_2$  nanorods and their good contact with the FTO substrate is favorable for electron transport.<sup>35</sup> The electrons of the  $\text{TiO}_2$  nanorods are transferred to the FTO substrate. Moreover, in contrast to the slow kinetic process between  $\text{TiO}_2$  and glucose oxidase, PDA is a p-type semiconductor<sup>18</sup> that induces a fast kinetic transfer at the interface between the glucose oxidase and PDA.<sup>36</sup> Hence, the photogenerated holes left in PDA can quickly transfer to glucose oxidase. Subsequently, glucose is oxidized to gluconic acid by glucose oxidase. The PDA shell in high HOMO level can avoid the oxidation and deactivation of enzymes. The mechanism proposed above is the basis for developing a stable inorganic/organic core/shell heterostructure-based PEC glucose biosensor with high sensitivity.

## 4. Conclusions

An excellent enzymatic glucose photoelectrochemical biosensor was constructed through the formation of  $\text{TiO}_2/\text{PDA}$  core/shell nanorod arrays, where PDA acts as a “bridge” to induce bidirectional quick transfers at the interfaces. Compared to the biosensor of  $\text{TiO}_2$  nanorod arrays, the PEC biosensor of the  $\text{TiO}_2/\text{PDA}$  core/shell displays a significantly enhanced photocurrent intensity and better performance in the detection of glucose. A remarkable performance with a sensitivity of 57.72  $\mu\text{A mM}^{-1} \text{ cm}^{-2}$ , a linear relationship range of 0.2–1 mM with a detection limit of 0.0285 mM ( $S/N = 3$ ) in the wide dynamic range of 1–6 mM, with a sensitivity of 8.75  $\mu\text{A mM}^{-1} \text{ cm}^{-2}$  were



obtained for glucose detection. PDA plays an important role in inducing the rapid transfer of photogenerated charge carriers at the interfaces of the TiO<sub>2</sub> and enzyme. Moreover, the PDA as shell do not only enhance the biosensor performance but also stabilizes it by avoiding the deactivation of enzymes resulting from the strong oxidative holes generated in TiO<sub>2</sub>. The core/shell structure with an excellent biocompatibility and effective separation efficiency of photogenerated carriers might be applied to other important biological interactions such as cell analysis.

## Conflicts of interest

There are no conflicts to declare.

## Acknowledgements

The authors thank Prof. Gang Liu (Institute of Metal Research, Chinese Academy of Sciences) for providing constructive and valuable suggestions on this work. This research was financially supported by the Key Research and Development Project of the Hainan Province (No. ZDYF2018106) and the National Natural Science Foundation of China (No. 51762012).

## Notes and references

- 1 J. Wang, *Chem. Rev.*, 2008, **108**, 814–825.
- 2 R. A. Doong and H. M. Shih, *Biosens. Bioelectron.*, 2010, **25**, 1439–1446.
- 3 P. Si, S. Ding, J. Yuan, X. W. Lou and D.-H. Kim, *ACS Nano*, 2011, **5**, 7617–7626.
- 4 W. W. Zhao, J. J. Xu and H. Y. Chen, *Chem. Soc. Rev.*, 2015, **44**, 729–741.
- 5 L. Wang, M. Wei, X. Gu, Y. Zhao and Y. Qiang, *J. Electron. Mater.*, 2018, **47**, 6540–6550.
- 6 K. Zhao, X. Yan, Y. Gu, Z. Kang, Z. Bai, S. Cao, Y. Liu, X. Zhang and Y. Zhang, *Small*, 2016, **12**, 245–251.
- 7 Z. Kang, X. Yan, Y. Wang, Y. Zhao, Z. Bai, Y. Liu, K. Zhao, S. Cao and Y. Zhang, *Nano Res.*, 2016, **9**, 344–352.
- 8 A. Fujishima and K. Honda, *Nature*, 1972, **238**, 37–38.
- 9 M. Dahl, Y. Liu and Y. Yin, *Chem. Rev.*, 2014, **114**, 9853–9889.
- 10 J. Bai and B. Zhou, *Chem. Rev.*, 2014, **114**, 10131–10176.
- 11 N. Smirnoff, *New Phytol.*, 1993, **125**, 27–58.
- 12 H. Huo, Z. Xu, T. Zhang and C. Xu, *J. Mater. Chem. A*, 2015, **3**, 5882–5888.
- 13 L. Guo, Z. Li, K. Marcus, S. Navarro, K. Liang, L. Zhou, P. D. Mani, S. J. Florczyk, K. R. Coffey, N. Orlovskaya, Y.-H. Sohn and Y. Yang, *ACS Sens.*, 2017, **2**, 621–625.
- 14 X. Liu, X. Huo, P. Liu, Y. Tang, J. Xu, X. Liu and Y. Zhou, *Electrochim. Acta*, 2017, **242**, 327–336.
- 15 W. Smith, A. Wolcott, R. C. Fitzmorris, J. Z. Zhang and Y. Zhao, *J. Mater. Chem.*, 2011, **21**, 10792–10800.
- 16 W. Li, A. Elzatahry, D. Aldhayan and D. Zhao, *Chem. Soc. Rev.*, 2018, **47**, 8203–8237.
- 17 C. Guo, H. Huo, X. Han, C. Xu and H. Li, *Anal. Chem.*, 2014, **86**, 876–883.
- 18 H. J. Nam, J. Cha, S. H. Lee, W. J. Yoo and D.-Y. Jung, *Chem. Commun.*, 2014, **50**, 1458–1461.
- 19 M. Zhao, Y. Gao, J. Sun and F. Gao, *Anal. Chem.*, 2015, **87**, 2615–2622.
- 20 H. Lee, S. M. Dellatore, W. M. Miller and P. B. Messersmith, *Science*, 2007, **318**, 426–430.
- 21 B. Yan, Y. Zhuang, Y. Jiang, W. Xu, Y. Chen, J. Tu, X. Wang and Q. Wu, *Appl. Surf. Sci.*, 2018, **458**, 382–388.
- 22 J. H. Bang and P. V. Kamat, *Adv. Funct. Mater.*, 2010, **20**, 1970–1976.
- 23 J. Li, X. Li, Q. Zhao, Z. Jiang, M. Tadé, S. Wang and S. Liu, *Sens. Actuators, B*, 2018, **255**, 133–139.
- 24 S.-C. Li, L.-N. Chu, X.-Q. Gong and U. Diebold, *Science*, 2010, **328**, 882–884.
- 25 S.-J. Bao, C. M. Li, J.-F. Zang, X.-Q. Cui, Y. Qiao and J. Guo, *Adv. Funct. Mater.*, 2008, **18**, 591–599.
- 26 D. R. Dreyer, D. J. Miller, B. D. Freeman, D. R. Paul and C. W. Bielawski, *Langmuir*, 2012, **28**, 6428–6435.
- 27 Y. Yang and W. Hu, *Talanta*, 2017, **166**, 141–147.
- 28 H. J. Nam, B. Kim, M. J. Ko, M. Jin, J. M. Kim and D.-Y. Jung, *Chem.-Eur. J.*, 2012, **18**, 14000–14007.
- 29 X. Kang, J. Wang, H. Wu, I. A. Aksay, J. Liu and Y. Lin, *Biosens. Bioelectron.*, 2009, **25**, 901–905.
- 30 B. Çakıroğlu and M. Özacar, *Biosens. Bioelectron.*, 2019, **141**, 111385.
- 31 J. C. Ndamani and L. Guo, *Bioelectrochemistry*, 2009, **77**, 60–63.
- 32 T. Rajh, L. X. Chen, K. Lukas, T. Liu, M. C. Thurnauer and D. M. Tiede, *J. Phys. Chem. B*, 2002, **106**, 10543–10552.
- 33 X. Zhou, B. Jin, J. Luo, X. Xu, L. Zhang, J. Li and H. Guan, *RSC Adv.*, 2016, **6**, 64446–64449.
- 34 F. Yu, S. Chen, Y. Chen, H. Li, L. Yang, Y. Chen and Y. Yin, *J. Mol. Struct.*, 2010, **982**, 152–161.
- 35 Q. Zhang, S. Yodyingyong, J. Xi, D. Myers and G. Cao, *Nanoscale*, 2012, **4**, 1436–1445.
- 36 G. Bagdžiūnas, Š. Žukauskas and A. Ramanavičius, *Biosens. Bioelectron.*, 2018, **102**, 449–455.
- 37 Z. Yang, Y. Ren, Y. Zhang, J. Li, H. Li, X. H. X. Hu and Q. Xu, *Biosens. Bioelectron.*, 2011, **26**, 4337–4341.
- 38 X. Zhang, M. Liu, H. Liu and S. Zhang, *Biosens. Bioelectron.*, 2014, **56**, 307–312.
- 39 Y. Wang, L. Liu, M. Li, S. Xu and F. Gao, *Biosens. Bioelectron.*, 2011, **30**, 107–111.
- 40 Z. Yang, Y. Tang, J. Li, Y. Zhang and X. Hu, *Biosens. Bioelectron.*, 2014, **54**, 528–533.
- 41 B. Çakıroğlu and M. Özacar, *Biosens. Bioelectron.*, 2018, **119**, 34–41.

